

Spin excitations in the heavily overdoped monolayer graphene superconductor: an analog to the cuprates

Wei-Jie Lin^{1,*}, W. LiMing^{1,*} and Tao Zhou^{1,2†}

¹Guangdong Provincial Key Laboratory of Quantum Engineering and Quantum Materials,
Department of Physics, School of Physics and Telecommunication Engineering,
South China Normal University, Guangzhou 510006, China

²Guangdong-Hong Kong Joint Laboratory of Quantum Matter,
Frontier Research Institute for Physics, South China Normal University, Guangzhou 510006, China

(Dated: February 23, 2021)

Recently it was reported experimentally that the monolayer graphene can be doped to beyond the Van Hove singularity. We study theoretically the possible superconductivity and the corresponding spin excitations of the monolayer graphene in this doping region. A static spin-density-wave state is favorable due to the nested Fermi surface as the Fermi level is doped to the Van Hove singularity point. Superconductivity may be realized upon further doping. The spin excitations in the superconducting state are studied theoretically based on the random phase approximation. The overall features are qualitatively the same with those in cuprate superconductors. Thus we have proposed an exciting possibility, namely, the heavily overdoped monolayer graphene can become a novel platform to study the unconventional superconductivity.

High- T_c superconductivity in the family of cuprate materials has been studied intensively for more than thirty years, while so far its mechanism remains puzzling [1]. This has motivated the great effort to seek for cuprate analogs. Previously, several possible candidate superconducting families have been proposed, including the iron-based superconductors [2] and the recently discovered nickelate superconductor [3].

The realization of superconductivity in graphene-based materials has been paid considerable attention since the first production of graphene in 2004 [4]. Previously, evidence of superconductivity has indeed been reported in several graphene-based materials with different methods [5–11]. Especially, it was reported that the twisted bilayer graphene will exhibit flat bands near the Fermi energy, leading to the correlated parent insulating states [12]. The superconductivity emerges upon doping electrons into this parent state. As a result, the twisted bilayer graphene has become a novel platform to study unconventional superconductivity and has attracted tremendous interest in the past several years [10].

The band structure of the monolayer graphene has saddle points at the M point of the Brillouin zone. The quasiparticle dispersion near this point is flat leading to the divergent density of states according the Van Hove singularity (VHS) scenario. Of particular interest is to tune the Fermi energy to the VHS point upon doping (the VHS filling) [13, 14]. Then the Fermi surface is perfectly nested leading to a spin-density-wave (SDW) instability [15–18]. On the other hand, the VHS near the Fermi level may provide an effective attractive potential then superconducting pairing is also favored [17–24]. Previously the competition between the SDW order and

the superconducting pairing has been studied theoretically [17, 18, 20]. Such competition is of interest and is indeed similar to that in the Cuprate compound.

Very recently, it was reported that the graphene doping technique reaches a new level, namely, the electron filling beyond the VHS filling was realized experimentally for the first time [25]. The electronic structure of the monolayer graphene at this doping region is similar to that of twisted graphene material [10–12]. At the VHS filling, the magnetic order is induced by the flat band at the Fermi energy. The static magnetic order is suppressed and the superconducting state may emerge upon further doping. Therefore, we expect that the monolayer may become another platform to study the unconventional superconductivity.

For cuprate superconducting materials, it is generally believed that spin excitations may play a fundamental role and mediate the superconducting pairing. Experimentally, the momentum and energy dependence of spin excitations are obtained directly through the inelastic neutron scattering (INS) experiments [26–32]. Theoretically, the INS experimental results can be compared through exploring the imaginary part of the dynamical spin susceptibility [33–37]. One of the most important results is the resonant spin excitation in the superconducting state [26–28, 33–37]. The spin resonance occurs at an energy proportional to the superconducting transition temperature [28, 35], so that it is believed to be intimately related to superconductivity. For the graphene-based material, previously it has been proposed theoretically that spin fluctuations may account for the superconductivity [23, 38]. Therefore, now it is timely and of importance to study the spin fluctuations in the superconducting monolayer graphene and compare the results with those in the high- T_c superconducting materials.

In this paper, we study theoretically the dynamic spin susceptibility of the mono-layer graphene material at the doping level beyond the VHS filling based on the random

* These two authors contributed equally to this work.

† Corresponding author: tzhou@scnu.edu.cn

phase approximation (RPA). We consider a typical $d+id$ pairing state, consistent with previous theoretical predictions [17–24]. The resonant spin excitation is indeed revealed. The overall features of spin excitations are qualitatively the same with those in high- T_c superconductors. Our results indicate that the mono-layer graphene materials are indeed analogous to the cuprate materials and may become a novel platform to study the mechanism of unconventional superconductivity.

We start from the Hamiltonian including the bare superconducting Hamiltonian and an onsite repulsive interaction, expressed as,

$$H = H_{\text{SC}} + H_{\text{int}}. \quad (1)$$

H_{SC} includes the hopping term and the superconducting pairing term. Considering the superconducting pairing between two nearest-neighbor sites, this term can be written as:

$$H_0 = -t \sum_{\langle ij \rangle, \sigma} (c_{i\sigma}^\dagger c_{j\sigma} + \text{h.c.}) + \sum_{\langle ij \rangle} (\Delta_{ij} c_{i\uparrow}^\dagger c_{j\downarrow}^\dagger + \text{h.c.}) - \mu \sum_{i, \sigma} c_{i\sigma}^\dagger c_{i\sigma}, \quad (2)$$

where \mathbf{j} is the nearest-neighbor site of the site \mathbf{i} with $\mathbf{j} = \mathbf{i} + \mathbf{e}_\alpha$. Here each site \mathbf{i} has three nearest-neighbor sites with $\mathbf{e}_1 = \frac{1}{2}(\sqrt{3}, 1)$, $\mathbf{e}_2 = \frac{1}{2}(-\sqrt{3}, 1)$ and $\mathbf{e}_3 = (0, -1)$. Δ_{ij} represents the superconducting pairing magnitude.

H_{int} is the on-site interaction term, expressed as

$$H_{\text{int}} = U \sum_{\mathbf{i}} n_{i\uparrow} n_{i\downarrow}. \quad (3)$$

In the momentum space, the bare Hamiltonian in the superconducting state can be expressed as a 4×4 lattice,

$$H_0(\mathbf{k}) = \begin{pmatrix} -\mu & f(\mathbf{k}) & 0 & \Delta(\mathbf{k}) \\ f^*(\mathbf{k}) & -\mu & \Delta(-\mathbf{k}) & 0 \\ 0 & \Delta^*(-\mathbf{k}) & \mu & -f^*(-\mathbf{k}) \\ \Delta^*(\mathbf{k}) & 0 & -f(-\mathbf{k}) & \mu \end{pmatrix}, \quad (4)$$

with $f(\mathbf{k}) = -t \sum_j e^{i\mathbf{k} \cdot \mathbf{e}_j}$ and $\Delta(\mathbf{k}) = \sum_j \Delta_j e^{i\mathbf{k} \cdot \mathbf{e}_j}$. For the $d+id$ pairing symmetry, we have $\Delta_{1,2,3} = \Delta_0 e^{i\frac{2}{3}\pi}$, $\Delta_0 e^{i\frac{4}{3}\pi}$, and Δ_0 .

The bare spin susceptibility from Eq.(4) can be written as a 4×4 matrix, with the elements including both the normal and the anomalous terms,

$$\chi_{l_3, l_2(0)}^{l_1, l_4}(\mathbf{q}, \omega) = \frac{1}{N} \sum_{\mathbf{k}} \sum_{\alpha, \beta=1}^4 [\xi_{l_1}^\alpha(\mathbf{k}) \xi_{l_2}^{\alpha,*}(\mathbf{k}) \xi_{l_3}^\beta(\mathbf{k} + \mathbf{q}) \xi_{l_4}^{\beta,*}(\mathbf{k} + \mathbf{q}) + \xi_{l_1}^\alpha(\mathbf{k}) \xi_{l_3+2}^{\alpha,*}(\mathbf{k}) \xi_{l_2}^{\beta,*}(\mathbf{k} + \mathbf{q}) \xi_{l_4+2}^\beta(\mathbf{k} + \mathbf{q})] \frac{f(E_{\mathbf{k}+\mathbf{q}}^\beta) - f(E_{\mathbf{k}}^\alpha)}{\omega + E_{\mathbf{k}}^\alpha - E_{\mathbf{k}+\mathbf{q}}^\beta + i\eta}, \quad (5)$$

where $l_i = 1, 2$ is the sublattice index of the graphene lattice. $E_{\mathbf{k}}^\alpha$ and $\xi^\alpha(\mathbf{k})$ are the eigenvalue and the eigenvector of the bare Hamiltonian $H(\mathbf{k})$. $f(x)$ is the Fermi distribution function.

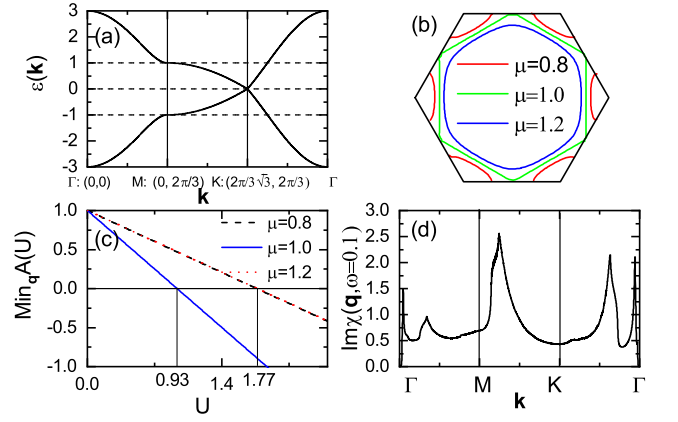


FIG. 1. (Color online) (a) The normal state energy bands along the highly symmetrical lines in the Brillouin zone. (b) The normal state Fermi surfaces with different chemical potentials. (c) The minimum value of the RPA factor as a function of the interaction U with $\omega = 0$. (d) The imaginary part of the renormalized normal state spin susceptibility as a function of the momentum with $\omega = 0.1$ and $\mu = 1.2$.

The renormalized spin susceptibility $\chi(\mathbf{q}, \omega)$ can be obtained through the RPA, given by

$$\hat{\chi}(\mathbf{q}, \omega) = [\hat{I} - \hat{\chi}_0(\mathbf{q}, \omega) \hat{U}]^{-1} \hat{\chi}_0(\mathbf{q}, \omega), \quad (6)$$

where \hat{I} is the 4×4 identity matrix. With onsite interaction being considered, the nonzero elements of the \hat{U} matrix include $U_{l_3, l_2}^{l_1, l_4} = U$ for $l_1 = l_2 = l_3 = l_4$. The physical spin susceptibility can be obtained through the sum of the elements of $\hat{\chi}$ with $l_1 = l_4$ and $l_2 = l_3$.

The normal state energy bands and Fermi surfaces [obtained by setting $\Delta_0 = 0$ in Eq.(4)] are displayed in Figs. 1(a) and 1(b), respectively. As is seen, at the M point [$\mathbf{Q}_M = (0, 2\pi/3)$], the quasiparticle dispersion is flat at the energy $E = 1.0$, leading to the VHS at this energy. When the chemical potential is below the VHS filling ($|\mu| < 1$), the normal state Fermi surface contains several small disconnected pockets. At the VHS filling with $\mu = 1$, the Fermi surface is perfectly nested. Beyond the VHS filling ($\mu > 1$), the Fermi surface is a large pocket centered at the $\Gamma = (0, 0)$ point.

As discussed previously [15–18], the nested Fermi surface will lead to the SDW instability. With the RPA framework, the SDW instability can be explored through the RPA factor $A(\mathbf{q}, \omega)$, with

$$A(\mathbf{q}, \omega) = \det | \hat{I} - \hat{\chi}_0(\mathbf{q}, \omega) \hat{U} |. \quad (7)$$

Generally at the zero energy the imaginary part of $A(\mathbf{q}, \omega)$ is zero. If its real part $\text{Re}A(\mathbf{q}, \omega = 0)$ at a certain wave-vector \mathbf{q} is negative, then the magnetic instability occurs. In this case the RPA method cannot be used directly and a static SDW order should be induced to describe the system. The minimum value of the RPA factor with $\omega = 0$ as a function of the onsite interaction U is plotted in Fig. 1(c). At the VHS filling ($\mu = 1.0$), $A(U)$ is

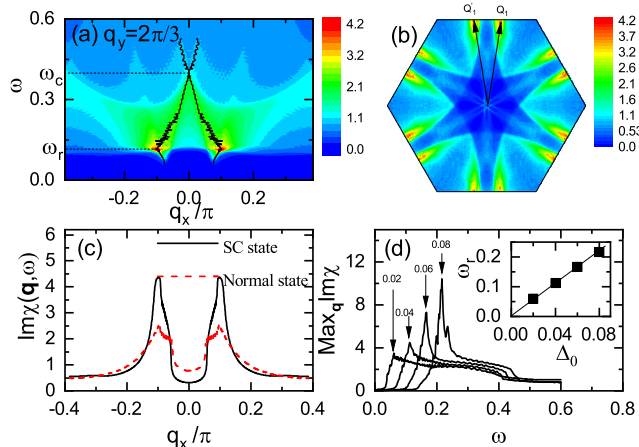


FIG. 2. (Color online) (a) The imaginary part of the spin susceptibility as functions of the energy and the momentum along the line $q_y = 2\pi/3$ with $\Delta_0 = 0.04$. (b) The imaginary part of the spin susceptibility as a function of the momentum with $\omega = \omega_r = 0.12$. (c) The imaginary parts of the spin susceptibility as a function of the momentum in the superconducting state and normal state with $\omega = \omega_r$. (d) The maximum value of $\text{Im}\chi(\mathbf{q}, \omega)$ in the Brillouin zone as a function of the energy with different gap magnitudes. Inset: The resonant energy ω_r as a function of the gap magnitude Δ_0 .

less than zero as the interaction U is larger than a critical value U_c ($U_c = 0.93$), indicating the signal for the SDW instability. As the chemical potential deviates from the VHS filling, this critical interaction U_c increases significantly. In the following presented results, we study the spin excitations beyond the VHS filling with $\mu = 1.2$ and $U = 1.6$. With these parameters the static SDW order disappears and the RPA technique is effective to study the spin fluctuation. The imaginary part of the renormalized normal state spin susceptibility as a function of the momentum with $\omega = 0.1$ is presented in Fig. 1(d). As is seen, the maximum spin excitation occurs at an incommensurate momentum ($\delta, 2\pi/3$) near the M point.

We now study the spin excitations in the superconducting state. The intensity plot of the imaginary part of the spin susceptibility ($\text{Im}\chi$) as functions of the energy and the momentum along the line $q_y = 2\pi/3$ with $\Delta_0 = 0.04$ is presented in Fig. 2(a). Here two typical energies, i.e., $\omega_r \approx 0.12$ and $\omega_c \approx 0.4$, are revealed and indicated in Fig. 2(a). At the energy ω_r , $\text{Im}\chi$ reaches its maximum value, at an incommensurate momentum with $\mathbf{q} = (\pm\delta, 2\pi/3)$. $\delta \approx 0.1\pi$ is the incommensurability. As the energy increases, the incommensurability decreases. At the energy ω_c , the spin excitation is commensurate with the maximum value appearing at the momentum $\mathbf{Q}_M = (0, 2\pi/3)$. As the energy increases to be larger than ω_c , the spin excitation becomes incommensurate again. The dispersion of the maximum spin excitations in the whole momentum and energy space has a hourglass shape.

Let us study in more detail the spin excitation at the

energy ω_r . The intensity plot of the imaginary part of the spin susceptibility in the whole Brillouin zone at the energy $\omega = \omega_r$ is displayed in Fig. 2(b). As is seen, the spin excitation has six-fold symmetry with the maximum excitation appearing at the incommensurate momenta \mathbf{Q}_1 and \mathbf{Q}'_1 (or their symmetrical momenta). The two dimensional cut of $\text{Im}\chi$ along the line $q_y = 2\pi/3$ as a function of q_x is replotted in Fig. 2(c). The imaginary part of the spin susceptibility in the normal state with $\omega = 0.12$ is also plotted in Fig. 2(c). As is seen, the intensity of the maximum $\text{Im}\chi$ at the energy ω_r in the superconducting state is significantly stronger than that in the normal state. The enhanced spin excitation in the superconducting state indicates the signal of the spin resonance. Previously, the resonant spin excitation has attracted broad interest in various unconventional superconductors [33–37]. It has been verified that the resonant energy is proportional to the gap magnitude or the superconducting transition temperature T_c [35]. The maximum spin excitations in the whole momentum space as a function of the energy with different gap magnitudes (from $\Delta_0 = 0.02$ to $\Delta_0 = 0.08$) are plotted in Fig. 2(d). The intensity of the maximum value of $\text{Im}\chi$ increases significantly as Δ_0 increases. The possible resonant energy ω_r can be obtained from Fig. 2(d) through the position of maximum $\text{Im}\chi$. The energy ω_r as a function of the gap magnitude is presented in the inset of Fig. 2(d). As is seen, here ω_r is proportional to Δ_0 . These features verify that the resonant spin excitation indeed exists in heavily overdoped superconducting graphene materials. This resonant spin excitation intimately related to the superconducting pairing. Such resonant behavior may be used to identify the unconventional superconductivity in this family.

We would like to compare the above numerical results of the spin excitation with those in high- T_c cuprate superconductors. In cuprate superconductors, the spin excitations are material dependent. For the La-based material (e.g., $\text{La}_{2-x}\text{Sr}_x\text{CuO}_4$), two energy scales are revealed experimentally [32]. The maximum spin excitation appears at a low energy about 18 meV and an incommensurate momentum. At a higher energy (about 50 meV), the spin excitation is commensurate. For Y-based high- T_c superconducting material (e.g., $\text{YBa}_2\text{Cu}_3\text{O}_{7-x}$), a resonant spin excitation at the energy about 40 meV is revealed [26, 27]. The spin excitation at this energy is commensurate. For both two materials, the dispersions have hourglass shape [29–32]. Here obviously, the spin excitations are analogous to those in La-based high- T_c superconducting materials, including the two energy scales and the hourglass shape dispersion. Moreover, we have checked numerically that if a rather strong gap magnitude is considered ($\Delta_0 \geq 0.2t$), the spin excitation at the resonant energy will become very strong and appears at the commensurate momentum \mathbf{Q}_M (the numerical results are not presented here). In this case the results are similar to those of Y-based superconductors. Therefore, our results indicate that the spin excitations in the doped su-

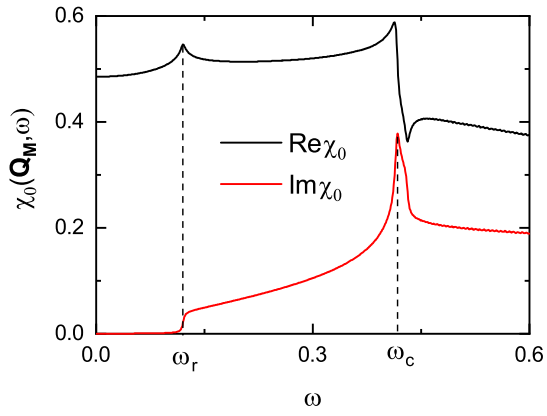


FIG. 3. (Color online) The real and imaginary parts of the bare spin susceptibility with $\Delta_0 = 0.04$.

perconducting graphene materials are indeed analogous to those in high- T_c cuprate superconductors.

The above features of spin excitations can be understood well based on the RPA framework and the topology of the Fermi surface. The general origin of the spin resonance in an unconventional superconductor has been studied intensively [33–37]. The renormalized spin susceptibility includes two parts of contributions, namely, the bare spin susceptibility $\chi_0(\mathbf{q}, \omega)$ and the RPA factor $A(\mathbf{q}, \omega)$. The real and imaginary parts of the bare spin susceptibility are displayed in Fig. 3. As is seen, the imaginary part of the bare spin susceptibility is nearly zero due to the presence of the spin gap. At the edge of the spin gap $\text{Im}\chi_0$ increases rapidly, then $\text{Re}\chi_0$ has a peak structure due to the Kramers-Kronig relation. As a result, the real part of the RPA factor reaches the minimum value at this energy. Thus the imaginary part of the renormalized spin susceptibility in the superconducting state will be enhanced at this energy, leading to the resonant spin excitation at this energy. At higher energies, the RPA factor plays minor role. The spin excitation is mainly determined by the bare spin susceptibility and the topology of the Fermi surface. The bare spin excitation has the maximum value at the energy ω_c , as indicated in Fig. 3. This can be understood further from the nesting of the energy contour.

The bare spin susceptibility is mainly contributed by a particle-hole excitation. Then we have $\text{Im}\chi_0(\mathbf{q}, \omega) \propto \sum_{\mathbf{k}} \delta[\omega - \Omega(\mathbf{q}, \mathbf{k})]$ with $\Omega(\mathbf{q}, \mathbf{k}) = E(\mathbf{k}) + E(\mathbf{k} + \mathbf{q})$. Generally, to explain the spin excitation at a certain energy ω_0 , one needs to study the scattering between the energy contour $\omega = \omega_0/2$ [33]. The contour plots of the energy contours with $E = \omega_r/2 = 0.06$ and $E = \omega_c/2 = 0.2$ in the first and extended Brillouin zones are presented in Fig. 4. As is seen, the contour $E = 0.06$ contains a flat piece, indicating the nesting feature. The best nesting vectors are indicated in Fig. 4, namely, \mathbf{Q}_1 and \mathbf{Q}'_1 , well consistent with the numerical results shown in Fig. 2. As the energy increases, the energy contours become larger. Naturally the incommensurability will decrease. As the

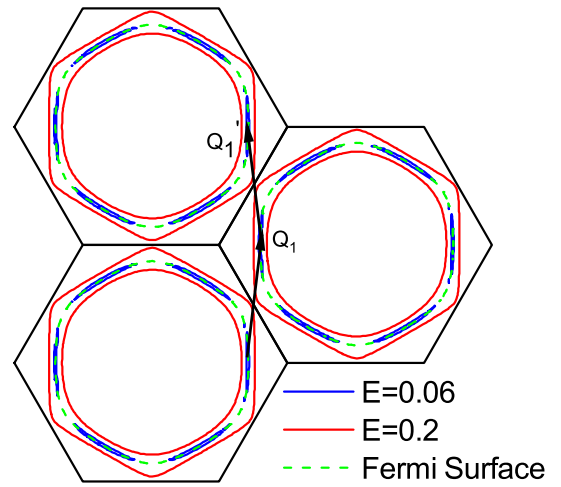


FIG. 4. (Color online) The constant energy contours with $E(\mathbf{k}) = 0.06$ and $E(\mathbf{k}) = 0.2$ in the first and extended Brillouin zone. The (green) dashed line is the normal state Fermi surface. The arrows indicate the nesting vectors for the contour $E(\mathbf{k}) = 0.06$.

energy is much greater than Δ_0 , the superconducting pairing term plays a minor role. As a result, the energy contours $E = 0.2$ are almost coincide with the normal state Fermi surfaces of $\mu = 1.0$ and $\mu = 1.4$. Since the normal state Fermi surface with $\mu = 1.0$ is perfectly nested with the nesting vector $\mathbf{q} = \mathbf{Q}_M$. As a result, the spin excitation at the energy $\omega = 0.4$ is commensurate and its maximum value appears at the momentum \mathbf{Q}_M . As the energy increases further, the nesting condition of the energy contour is broken and the spin excitation will become incommensurate again.

At last, we summarize the similarity between the possible superconductivity in heavily overdoped graphene material with that in cuprates. Firstly, the general phase diagram may be similar. For the graphene material, at the VHS filling, the Fermi surface is nested, leading to the SDW instability. Beyond the VHS filling, the static SDW order is suppressed and the superconductivity may emerge. For the cuprates, at the half-filling, the system is in the antiferromagnetic state. Upon doping the antiferromagnetic order is suppressed and the superconductivity is realized. Secondly, although so far no consensus has been reached about the mechanism of superconductivity in cuprates, while many believe that spin fluctuation should play essential role. Here for the heavily overdoped graphene material, strong spin fluctuation should exist due to the nesting of the Fermi surface. Such strong fluctuation could account for possible unconventional superconductivity graphene materials. Thirdly, as presented in our present work, the overall features of spin excitations in superconducting graphene materials are qualitatively similar with those of cuprate superconductors, including the resonant spin excitation at a certain energy and the hourglass dispersions. Therefore, here we propose that the highly overdoped monolayer graphene material may

be a potential candidate to be the cuprate analog.

In conclusion, we have studied theoretically spin excitations in the superconducting state of the monolayer graphene material beyond the VHS filling. Two typical energies are revealed. At a low energy, a resonant spin excitation is revealed at an incommensurate momentum. At a higher energy, the spin excitation is commensurate. The dispersion of the spin excitation has a hourglass shape. The overall features are qualitatively the same

with those in superconducting cuprate materials. We propose that the mono-layer graphene beyond the VHS filling are candidate to become cuprate analogs. All of the results can be used to identify the unconventional superconductivity in this compound.

This work was supported by the NSFC (Grant No. 12074130) and Science and Technology Program of Guangzhou (Grant No. 2019050001).

-
- [1] P. A. Lee, N. Nagaosa, and X.-G. Wen, Doping a mott insulator: Physics of high-temperature superconductivity, *Rev. Mod. Phys.* **78**, 17 (2006).
- [2] G. R. Stewart, Superconductivity in iron compounds, *Rev. Mod. Phys.* **83**, 1589 (2011).
- [3] D. Li, K. Lee, B. Y. Wang, M. Osada, S. Crossley, H. R. Lee, Y. Cui, Y. Hikita, and H. Y. Hwang, Superconductivity in an infinite-layer nickelate, *Nature* **572**, 624 (2019).
- [4] A. H. Castro Neto, F. Guinea, N. M. R. Peres, K. S. Novoselov, and A. K. Geim, The electronic properties of graphene, *Rev. Mod. Phys.* **81**, 109 (2009).
- [5] C. Tonnoir, A. Kimouche, J. Coraux, L. Magaud, B. Delsol, B. Gilles, and C. Chapelier, Induced superconductivity in graphene grown on rhenium, *Phys. Rev. Lett.* **111**, 246805 (2013).
- [6] S. Ichinokura, K. Sugawara, A. Takayama, T. Takahashi, and S. Hasegawa, Superconducting calcium-intercalated bilayer graphene, *ACS Nano* **10**, 2761 (2016).
- [7] J. Chapman, Y. Su, C. Howard, D. Kundys, A. Grigorenko, F. Guinea, A. Geim, I. Grigorieva, and R. Nair, Superconductivity in ca-doped graphene laminates, *Sci. rep.* **6**, 23254 (2016).
- [8] A. Di Bernardo, O. Millo, M. Barbone, H. Alpern, Y. Kalcheim, U. Sassi, A. K. Ott, D. De Fazio, D. Yoon, M. Amado, A. C. Ferrari, J. Linder, and J. W. A. Robinson, p-wave triggered superconductivity in single-layer graphene on an electron-doped oxide superconductor, *Nat. Commun.* **8**, 14024 (2017).
- [9] B. M. Ludbrook, G. Levy, P. Nigge, M. Zonno, M. Schneider, D. J. Dvorak, C. N. Veenstra, S. Zhdanovich, D. Wong, P. Dosanjh, C. Straßer, A. Stöhr, S. Forti, C. R. Ast, U. Starke, and A. Damascelli, Evidence for superconductivity in li-decorated monolayer graphene, *Proc. Natl. Acad. Sci. U. S. A.* **112**, 11795 (2015).
- [10] Y. Cao, V. Fatemi, S. Fang, K. Watanabe, T. Taniguchi, E. Kaxiras, and P. Jarillo-Herrero, Unconventional superconductivity in magic-angle graphene superlattices, *Nature* **556**, 43 (2018).
- [11] J. M. Park, Y. Cao, K. Watanabe, T. Taniguchi, and P. Jarillo-Herrero, Tunable strongly coupled superconductivity in magic-angle twisted trilayer graphene, *Nature* **590**, 249 (2021).
- [12] Y. Cao, V. Fatemi, A. Demir, S. Fang, S. L. Tomarken, J. Y. Luo, J. D. Sanchez-Yamagishi, K. Watanabe, T. Taniguchi, E. Kaxiras, R. C. Ashoori, and P. Jarillo-Herrero, Correlated insulator behaviour at half-filling in magic-angle graphene superlattices, *Nature* **556**, 80 (2018).
- [13] P. Rosenzweig, H. Karakachian, S. Link, K. Küster, and U. Starke, Tuning the doping level of graphene in the vicinity of the van hove singularity via ytterbium intercalation, *Phys. Rev. B* **100**, 035445 (2019).
- [14] S. Link, S. Forti, A. Stöhr, K. Küster, M. Rösner, D. Hirschmeier, C. Chen, J. Avila, M. C. Asensio, A. A. Zakharov, T. O. Wehling, A. I. Lichtenstein, M. I. Katsnelson, and U. Starke, Introducing strong correlation effects into graphene by gadolinium intercalation, *Phys. Rev. B* **100**, 121407 (2019).
- [15] T. Li, Spontaneous quantum hall effect in quarter-doped hubbard model on honeycomb lattice and its possible realization in doped graphene system, *Europhys. Lett.* **97**, 37001 (2012).
- [16] D. Makogon, R. van Gelderen, R. Roldán, and C. M. Smith, Spin-density-wave instability in graphene doped near the van hove singularity, *Phys. Rev. B* **84**, 125404 (2011).
- [17] W.-S. Wang, Y.-Y. Xiang, Q.-H. Wang, F. Wang, F. Yang, and D.-H. Lee, Functional renormalization group and variational monte carlo studies of the electronic instabilities in graphene near $\frac{1}{4}$ doping, *Phys. Rev. B* **85**, 035414 (2012).
- [18] M. L. Kiesel, C. Platt, W. Hanke, D. A. Abanin, and R. Thomale, Competing many-body instabilities and unconventional superconductivity in graphene, *Phys. Rev. B* **86**, 020507 (2012).
- [19] S. Pathak, V. B. Shenoy, and G. Baskaran, Possible high-temperature superconducting state with a $d + id$ pairing symmetry in doped graphene, *Phys. Rev. B* **81**, 085431 (2010).
- [20] J. L. McChesney, A. Bostwick, T. Ohta, T. Seyller, K. Horn, J. González, and E. Rotenberg, Extended van hove singularity and superconducting instability in doped graphene, *Phys. Rev. Lett.* **104**, 136803 (2010).
- [21] R. Nandkishore, L. S. Levitov, and A. V. Chubukov, Chiral superconductivity from repulsive interactions in doped graphene, *Nat. Phys.* **8**, 158 (2012).
- [22] R. Nandkishore, R. Thomale, and A. V. Chubukov, Superconductivity from weak repulsion in hexagonal lattice systems, *Phys. Rev. B* **89**, 144501 (2014).
- [23] L.-Y. Xiao, S.-L. Yu, W. Wang, Z.-J. Yao, and J.-X. Li, Possible singlet and triplet superconductivity on honeycomb lattice, *Europhys. Lett.* **115**, 27008 (2016).
- [24] F. Xu and L. Zhang, Unconventional chiral d-wave superconducting state in strained graphene, *Chin. Phys. B* **28**, 117403 (2019).
- [25] P. Rosenzweig, H. Karakachian, D. Marchenko, K. Küster, and U. Starke, Overdoping graphene beyond the van hove singularity, *Phys. Rev. Lett.* **125**, 176403 (2020).

- [26] J. Rossat-Mignod, L. Regnault, C. Vettier, P. Bourges, P. Burllet, J. Bossy, J. Henry, and G. Lapertot, Neutron scattering study of the $\text{YBa}_2\text{Cu}_3\text{O}_{6+x}$ system, *Physica C* **185-189**, 86 (1991).
- [27] J. M. Tranquada, P. M. Gehring, G. Shirane, S. Shamoto, and M. Sato, Neutron-scattering study of the dynamical spin susceptibility in $\text{YBa}_2\text{Cu}_3\text{O}_{6.6}$, *Phys. Rev. B* **46**, 5561 (1992).
- [28] H. He, Y. Sidis, P. Bourges, G. D. Gu, A. Ivanov, N. Koshizuka, B. Liang, C. T. Lin, L. P. Regnault, E. Schoenherr, and B. Keimer, Resonant spin excitation in an overdoped high temperature superconductor, *Phys. Rev. Lett.* **86**, 1610 (2001).
- [29] M. Arai, T. Nishijima, Y. Endoh, T. Egami, S. Tajima, K. Tomimoto, Y. Shiohara, M. Takahashi, A. Garrett, and S. M. Bennington, Incommensurate spin dynamics of underdoped superconductor $\text{YBa}_2\text{Cu}_3\text{O}_{6.7}$, *Phys. Rev. Lett.* **83**, 608 (1999).
- [30] P. Bourges, Y. Sidis, H. F. Fong, L. P. Regnault, J. Bossy, A. Ivanov, and B. Keimer, The spin excitation spectrum in superconducting $\text{YBa}_2\text{Cu}_3\text{O}_{6.85}$, *Science* **288**, 1234 (2000).
- [31] S. M. Hayden, H. A. Mook, P. Dai, T. G. Perring, and F. Doğan, The structure of the high-energy spin excitations in a high-transition-temperature superconductor, *Nature* **429**, 531 (2004).
- [32] B. Vignolle, S. M. Hayden, D. F. McMorrow, H. M. Rønnow, B. Lake, C. D. Frost, and T. G. Perring, Two energy scales in the spin excitations of the high-temperature superconductor $\text{La}_{2-x}\text{Sr}_x\text{CuO}_4$, *Nat. Phys.* **3**, 163 (2007).
- [33] J. Brinckmann and P. A. Lee, Slave boson approach to neutron scattering in $\text{YBa}_2\text{Cu}_3\text{O}_{6+y}$ superconductors, *Phys. Rev. Lett.* **82**, 2915 (1999).
- [34] Y. Gao, Y. Yu, T. Zhou, H. Huang, and Q.-H. Wang, Possible spin excitation structure in monolayer FeSe grown on SrTiO_3 , *Phys. Rev. B* **96**, 014515 (2017).
- [35] T. Zhou and Z. D. Wang, Phenomenological theory of spin excitations in La- and Y-based cuprates, *Phys. Rev. B* **76**, 094510 (2007).
- [36] J.-X. Li and Z. D. Wang, Spin-resonance peak in $\text{Na}_x\text{CoO}_2 \cdot y\text{H}_2\text{O}$ superconductors: A probe of the pairing symmetry, *Phys. Rev. B* **70**, 212512 (2004).
- [37] T. Zhou, Y. Gao, and Z. Wang, Spin excitations in nickelate superconductors, *Sci. China-Phys. Mech. Astron.* **63**, 287412 (2020).
- [38] A. Fischer, L. Klebl, C. Honerkamp, and D. M. Kennes, Spin-fluctuation-induced pairing in twisted bilayer graphene, *Phys. Rev. B* **103**, L041103 (2021).